Spatial Statistics 19 (2017) 1–20

Contents lists available at ScienceDirect

Spatial Statistics

journal homepage: www.elsevier.com/locate/spasta

Median Polish Kriging for space–time analysis of precipitation

William A. Martínez [a,*], Carlos E. Melo [a], Oscar O. Melo [b]

[a] Faculty of Engineering, Universidad Distrital Francisco José de Caldas, Bogotá, Cra 7 No 40B-53, Colombia

[b] Department of Statistics, Faculty of Sciences, Universidad Nacional de Colombia, Bogotá, Cra 45 No 26-85, Colombia

ARTICLE INFO

Article history:
Received 22 November 2015
Accepted 17 October 2016
Available online 22 November 2016

Keywords:
Correlation space–time model
Median polish
Precipitation
Space–time kriging

ABSTRACT

According to Cressie (1991), the median polish kriging (MPK) is a hybrid method for predicting of spatial data in a two dimensional surface. It combines a kriging interpolator and an analysis of tables. As a result of the effect of a directional trend that models the orographic structure at a specific place, and the periodic temporal character associated with an atmospheric process, such as rainfall, an extension to the number of exploration dimensions is proposed by using median polish in an additive approach, for one temporal and three spatial dimensions (latitude, longitude and altitude). In this sense, after applying an outlier resistant and robust prediction method as the MPK, the stationary on residuals was ideal to estimate the structure covariance function, which was obtained fitting a sum–product model with a spatial exponential effect and a hole-effect without dampening in time. The spatio-temporal modified MPK was used for mapping of monthly precipitation, based on 102 irregularly spaced weather stations from Colombia, for the period 2000–2010. The functional form was adapted to spatial–temporal kriging to create monthly precipitations maps for wettest and driest periods, and a forecast for the rainiest period in the year 2010. Finally, the accuracy of the method was assessed through a cross validation analysis.

* Corresponding author.
E-mail addresses: willimarti2008@gmail.com (W.A. Martínez), cmelo@udistrital.edu.co (C.E. Melo), oomelom@unal.edu.co (O.O. Melo).

http://dx.doi.org/10.1016/j.spasta.2016.10.003
2211-6753/

1. Introduction

In recent years, the enormous growth of data having spatio-temporal structure has generated a considerable interest in the development of spatio-temporal models, in areas such as meteorology, epidemiology and environmental sciences. Nevertheless, the complexity of fitting models and the size of data sets pose a challenge. The analysis of rainfall amounts in equatorial highlands led to the development of the methodology presented in this paper. It considers the space–time coordinates as the main covariates of precipitation, and the use of a suitable model to estimate simultaneously spatial and temporal trends.

Classic geostatistics is based on spatio-temporal processes subject to some kind of stationary (Cressie and Wikle, 2011), but real processes rarely obey this condition over large areas and different time intervals, so non-stationarity is limited to a trend component, which is modeled like a space–time function (Martínez-Ruiz, 2008). However, the trend is not completely removed, and spatial association can be altered by linear trend models (Berke, 2001). In order to consider the data as following a normal with mean and variance constants without a trend in the study directions, Cressie (1991) proposed a synergy of ordinary kriging with the technique of exploration and analysis of tables developed by Tukey (1977), called median polish (Hoaglin et al., 2000) for interpolation of spatial data.

From an exploratory perspective, the data decomposition in multidimensional arrays is possible, so the relations of a quantitative response variable as a function of a set of independent variables can be examined (Hoaglin et al., 2011). In the context of spatial statistics, the median polish technique is built on two dimensional arrays (see Rekabi and El Sheikh, 2013 and Berke, 2004). On the other hand, if the measurements have a three-dimensional structure adapted to the geographical relief of any place with rows, columns and layers that represent the directions of a three-dimensional system, the contribution of the three factors can be visualized on the variable. This scheme was introduced by Mohanty and Kanwar (1994), who explored the variability of nitrate and nitrogen residual data with spatial regularity in east and north directions and soil depth, and showed the advantages of this method in processes for which the dimension of Z may be also associated with an additional pattern of phenomenon variability.

As described above, there are many ways to integrate a function over an irregular data. The works of Luo et al. (1998) and Lee and Durbán (2011) show a methodology for spatio-temporal data that uses smoothing spline models and analysis of variance (ANOVA), integrating solutions by interactions and handling large amounts of irregular data with variations in space and time. Their work forms the basis for our proposed methodology. However, our work includes a structural analysis through which a covariance and a trend degree to the response variable under study are fitted.

Furthermore, the median polish technique has been implemented in spatial data analysis with progression in time; Sun and Genton (2012) proposed a comparison between the ANOVA and the median polish with a bivariate view by categorizing space climatic regions and using data on precipitation and temperature. Their comparison shows the robustness of MPK method with respect to a classical factorial analysis.

Taking into account the above characteristics, we extend the dimension in the median polish technique, considering a four-way analysis for a regionalized response variable in space–time, which allows to see the factors influence in a dynamic process on four dimensions, and to validate the stationary residuals. To get it, we implemented the STMedianPolish library of the R package (Martinez et al., 2015), in order to create a spatio-temporal object with regular data for using median polish technique and for estimating the trend surface, so that, the variogram that represents the spatial and temporal correlation structure data can be estimated. However, there is not uncertainty assessment in MPK, as the uncertainty in the mean component is not quantified by the median polish procedure but only the uncertainty in the interpolation of the residuals.

This paper describes in Section 2 the algorithm of MPK in four-way data structure, the application of the method on monthly precipitation data in Section 3, and conclusions in Section 4.

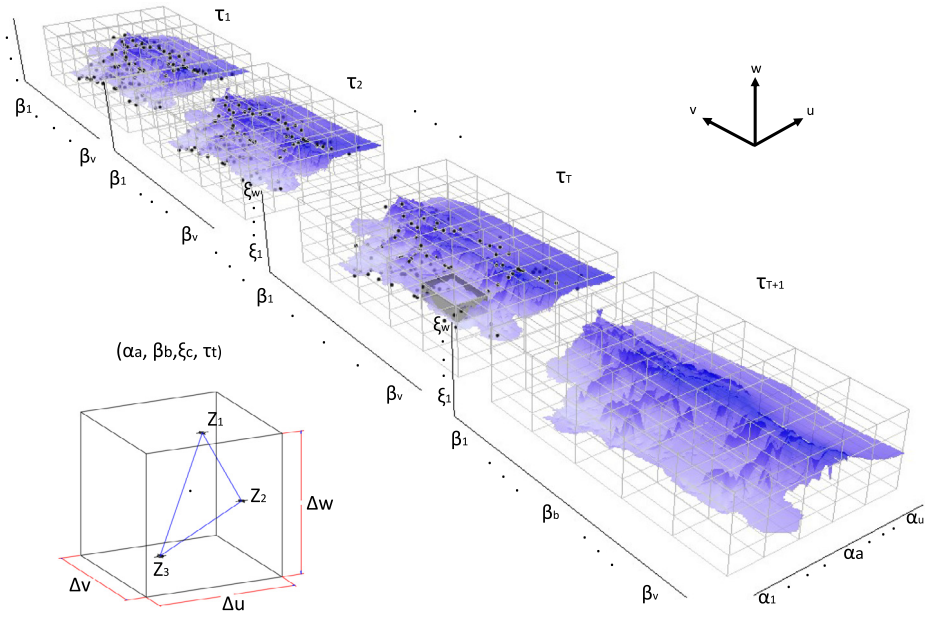

Fig. 1. Spatial–temporal median polish setting.

2. Median polish kriging

In this section, the fundamentals of the theory of MPK are explained in four-way data structure, and sample data that are not distributed regularly in space are also described.

2.1. Factorial design for space–time process

The main objective will be an analysis of a given spatio-temporal process $\{Z(\mathbf{s}, t), \mathbf{s} \in \mathfrak{D}, t \in \mathfrak{T}\}$, defined as a set of dependent random variables where the spatial index $\mathbf{s}$ varies in $\mathfrak{D} \subseteq \mathbb{R}^3$, and the temporal index t in $\mathfrak{T} \subseteq \mathbb{Z}$. This process can be decomposed as:

$$Z(\mathbf{s}, t) = \mu(\mathbf{s}, t) + \delta(\mathbf{s}, t) \tag{1}$$

where $\mu(\cdot)$ denotes the spatio-temporal deterministic component, and $\delta(\cdot)$ is the stochastic residual component, which represents the random fluctuations of the process. Under this structure, Berke's approach (Berke, 2001) for MPK is implemented for irregularly spaced data, extending the analysis of a structure from two dimensions to a structure in four dimensions (with $U \times V \times W$ cells and T temporal scenarios).

In this paper, we assume that the above four dimensions contribute by separate and in an additive form to the response variable. If we arrange the data in a four-dimensional array, we expect to visualize these contributions as rows, columns, layers, and time (see Fig. 1).

Thus, let α_a, β_b, ξ_c and τ_t be the row, column, layer and time factors, respectively, with U, V, W and T levels, respectively. All factor combinations are $U \times V \times W \times T$, which under a distribution of irregularly spaced data would generate a cell with different amounts of observations, and even empty cells (see Fig. 2).

When we configure an irregular distribution of spatial data in two-ways tables (see Fig. 2 (left)), we hope that the response variable will be a function of two factors (row and column), a constant term, and fluctuations around the response variable (noises); furthermore, an interaction between both factors may even be added, which could translate into a trend in a direction that is not orthogonal. This model requires only two-dimensional position for the observation. However, there are cases where

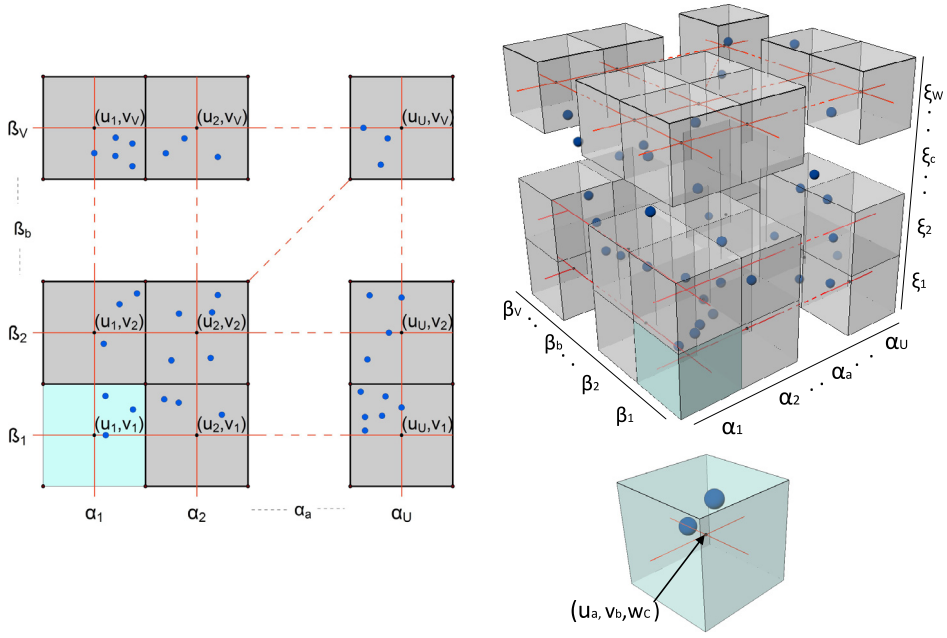

Fig. 2. Decomposition in two dimensions (left) and decomposition in three dimensions (right).

the response variable also can be influenced by a factor of altitude; for example, the precipitation or temperature in mountainous regions (see Fig. 2 (right)). Then, each observation that we saw in two dimensions can be displayed with its respective elevation in three dimensions.

In respect to the network of sample sites, MPK with irregular distributed geostatistical data is achieved defining a $U \times V \times W \times t$ rectangular box on time grid to be laid over an investigation region. Furthermore, the sample data $Z(\mathbf{s}_i, t)$, $i = 1, \ldots, n$ and $t = 1, \ldots, T$ are aligned with the closest grid knots $(\mathbf{s}_{abc}, t)$, $a = 1, \ldots, U$, $b = 1, \ldots, V$, $c = 1, \ldots, W$, and the coordinates of the sample sites $(\mathbf{s}_i, t)$ are converted to that of the corresponding grid lines $(\mathbf{s}_{abc}, t)$, so $\mathbf{s}_i = (u_a, v_b, w_c)$. For multiple data aligned with a single grid knot, the data is replaced by the median. Therefore, the edited sample data, say $Y(\mathbf{s}_{abc}, t)$, have the structure of a four-way table and are suitable for median polishing. Median polishing proceeds by repeated extraction of the rectangular box on time medians until it converges, based on a stopping criterion to be chosen by the investigator.

According to the above, the space division is an issue of special importance when dealing with irregularly spaced data because it will define the map resolution trend, and it will seek to reduce systematic occurrences of missing values within each cell. Along these lines, we propose to evaluate empirically the performance of the median of all distances between stations in each direction of the spatial arrangement.

Fig. 3 shows the deltas among stations for which the next matrix of distances, for axis u distribution, is constructed:

$$\begin{pmatrix} \Delta u_{11} & \Delta u_{12} & \cdots & \Delta u_{1i} & \cdots & \Delta u_{1n} \\ \Delta u_{21} & \Delta u_{22} & \cdots & \Delta u_{2i} & \cdots & \Delta u_{2n} \\ \vdots & \vdots & \ddots & \vdots & \ddots & \vdots \\ \Delta u_{i1} & \Delta u_{i2} & \cdots & \Delta u_{ii} & \cdots & \Delta u_{in} \\ \vdots & \vdots & \ddots & \vdots & \ddots & \vdots \\ \Delta u_{n1} & \Delta u_{n2} & \cdots & \Delta u_{ni} & \cdots & \Delta u_{nn} \end{pmatrix}.$$

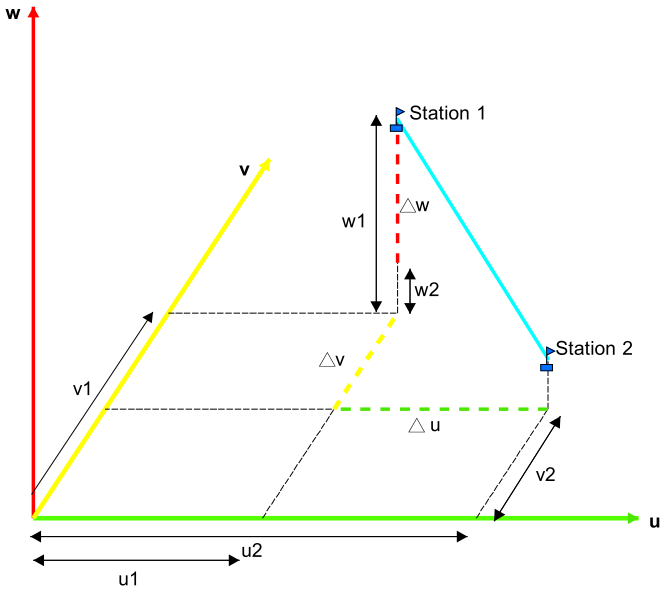

Fig. 3. Distances to the axes of two stations of precipitation.

For each station in the study domain, each column contains the distances on all its neighbors in the u axis direction. Once built, the median is extracted by column such that the smallest medium will correspond to the number of columns in the spatial arrangement. Therefore, Δu is given by

$$\Delta u = \min\left[\text{med}\left(\{\Delta u_{i1} : i = 1, \ldots, n\}\right), \ldots, \text{med}\left(\{\Delta u_{i2} : i = 1, \ldots, n\}\right), \ldots, \text{med}\left(\{\Delta u_{in} : i = 1, \ldots, n\}\right)\right] \tag{2}$$

where med denotes the median.

Similarly, the distances are obtained for the v and w axes that must be divided into the study domain. In this sense, the cells with multiple data will take the average value of the data (Luo et al., 1998). In the same way, Berke (2001) suggests median according to the MPK method that also uses median on rows–columns. Finally, the sample data, $Y(\mathbf{s}_{abc}, t)$, have a four-way structure for implementing of the median polish.

2.2. Spatio-temporal prediction: median polish kriging

Although the trend $\mu(\mathbf{s}, t)$ may be associated with any spatio-temporal direction, including interactions between the axes, this study keeps in a simple form the decomposition of four factors that exert a separate and additive influence on the variable.

Following the Berke's approach (Berke, 2001) but now using a structure in four dimensions, median polishing proceeds by repeated extraction of the row, column, layer and time medians until convergence, with respect to a stopping criterion to be chosen by the investigator. A mathematical formulation of the median polish algorithm is given in Cressie (1991) and Berke (2001). For data $\{Y(\mathbf{s}_{abc}, t), a = 1, \ldots, U, b = 1, \ldots, V, c = 1, \ldots, W, t = 1, \ldots, T, \mathbf{s}_{abc} \in \mathfrak{D}, t \in \mathfrak{T}\}$, so a spatial and temporal process is given by:

$$Y(\mathbf{s}_{abc}, t) = \mu_y(\mathbf{s}_{abc}, t) + \delta_{abct} \tag{3}$$

where

$$\mu_y(\mathbf{s}_{abc}, t) = \mu + \alpha_a + \beta_b + \xi_c + \tau_t, \tag{4}$$

and δ_{abct} is the fluctuation arising from a natural variability and from the measurement process. Additionally, μ is an overall mean, α_a is the ath row effect, β_b is the bth column effect, ξ_c is the cth layer effect, and τ_t is the tth time effect.

Thus, the next step is to remove the effects of each level (a, b, c and t). The median polish requires several iterations until the following conditions are met:

$$\underset{a}{\text{med}}\{\alpha_a\} = \underset{b}{\text{med}}\{\beta_b\} = \underset{c}{\text{med}}\{\xi_c\} = \underset{t}{\text{med}}\{\tau_t\} = 0.$$

This condition is analogous to the usual conditions in analysis of variance, i.e.

$$\sum_a \alpha_a = \sum_b \beta_b = \sum_c \xi_c = \sum_t \tau_t = 0.$$

2.3. Algorithmic representation

In this section, we illustrate the procedure algebraically. First, we let a parenthesized superscript denote the number of the iterative cycle to establish notation. So, $A_a^{(m)}$, $B_b^{(m)}$, $C_c^{(m)}$ and $F_t^{(m)}$ denote the median estimated effects of the various levels of factors row, column, layer and time, respectively, removed in cycle m. Later, we add these up over cycles and take care of any necessary centering. At the start of the procedure we may assign

$$A_a^{(0)} = B_b^{(0)} = C_c^{(0)} = F_t^{(0)} = 0, \quad \text{for all } a, b, c, t.$$

If the $r_{abct}^{(m)}$'s are the residuals after taking out the row, column, layer, and time effects in cycle m, then we can start with $r_{abct}^{(0)} = y_{abct}$, which are the original data. Now the details of the iteration are examined, removing medians in the order: row, column, layer, and time, but in practice any order would do. Sometimes the results depend a little on the order chosen.

The ν ($\nu = 1, \ldots, m$) cycle proceeds as follows: First, the median is taken for each level of factor row,

$$A_a^{(\nu)} = \underset{bct}{\text{med}}\left\{r_{abct}^{(\nu-1)}\right\}, \quad a = 1, \ldots, U$$

the median over all b, c and t, holding a fixed. Next, these medians are subtracted from the $r_{abct}^{(\nu-1)}$ and new median is taken for each level of factor column,

$$B_b^{(\nu)} = \underset{act}{\text{med}}\left\{r_{abct}^{(\nu-1)} - A_a^{(\nu)}\right\}, \quad b = 1, \ldots, V.$$

Then, these $B_b^{(1)}$'s are subtracted and the median is taken for each level of factor layer,

$$C_c^{(\nu)} = \underset{abt}{\text{med}}\left\{r_{abct}^{(\nu-1)} - A_a^{(\nu)} - B_b^{(\nu)}\right\}, \quad c = 1, \ldots, W$$

and then, these $C_c^{(1)}$'s are subtracted and the median is taken for each level of factor time,

$$F_t^{(\nu)} = \underset{abc}{\text{med}}\left\{r_{abct}^{(\nu-1)} - A_a^{(\nu)} - B_b^{(\nu)} - C_c^{(\nu)}\right\}, \quad t = 1, \ldots, T.$$

Subtracting these $F_t^{(\nu)}$ yields the residuals

$$r_{abct}^{(\nu)} = r_{abct}^{(\nu-1)} - A_a^{(\nu)} - B_b^{(\nu)} - C_c^{(\nu)} - F_t^{(\nu)}.$$

If we wish to center the effect estimates at this stage, the median of each set of effects is taken and then, the effect estimates are given by:

$$
\begin{aligned}
\hat{\alpha}_a &= \sum_{\nu=1}^{m} A_a^{(\nu)} - \underset{a}{\text{med}} \left\{ \sum_{\nu=1}^{m} A_a^{(\nu)} \right\}, \quad a = 1, \ldots, U \\
\hat{\beta}_b &= \sum_{\nu=1}^{m} B_b^{(\nu)} - \underset{b}{\text{med}} \left\{ \sum_{\nu=1}^{m} B_b^{(\nu)} \right\}, \quad b = 1, \ldots, V \\
\hat{\xi}_c &= \sum_{\nu=1}^{m} C_c^{(\nu)} - \underset{c}{\text{med}} \left\{ \sum_{\nu=1}^{m} C_c^{(\nu)} \right\}, \quad c = 1, \ldots, W \\
\hat{\tau}_t &= \sum_{\nu=1}^{m} F_t^{(\nu)} - \underset{t}{\text{med}} \left\{ \sum_{\nu=1}^{m} F_t^{(\nu)} \right\}, \quad t = 1, \ldots, T \\
\hat{\mu} &= \underset{a}{\text{med}} \left\{ \sum_{\nu=1}^{m} A_a^{(\nu)} \right\} + \underset{b}{\text{med}} \left\{ \sum_{\nu=1}^{m} B_b^{(\nu)} \right\} + \underset{c}{\text{med}} \left\{ \sum_{\nu=1}^{m} C_c^{(\nu)} \right\} + \underset{t}{\text{med}} \left\{ \sum_{\nu=1}^{m} F_t^{(\nu)} \right\}.
\end{aligned} \tag{5}
$$

These final estimates depend somewhat on the order used in taking medians, but typically not enough to be of much practical importance. In practice, we usually carry out a fixed number of iterations, at least two or three, and use this as our standard analysis. In this four-way median-polish procedure, the calculations are guided to approach the side conditions or "complete removal" conditions

$$
\begin{aligned}
&\underset{bct}{\text{med}} \{r_{abct}\} = 0 \quad \text{for each } a, \qquad \underset{act}{\text{med}} \{r_{abct}\} = 0 \quad \text{for each } b, \\
&\underset{abt}{\text{med}} \{r_{abct}\} = 0 \quad \text{for each } c, \qquad \underset{abc}{\text{med}} \{r_{abct}\} = 0 \quad \text{for each } t, \\
&\underset{a}{\text{med}}\{\hat{\alpha}_a\} = 0, \qquad \underset{b}{\text{med}}\{\hat{\beta}_b\} = 0, \qquad \underset{a}{\text{med}}\{\hat{\xi}_c\} = 0, \qquad \underset{a}{\text{med}}\{\hat{\tau}_t\} = 0.
\end{aligned}
$$

These show that nothing remains to take out, at least in median terms.

2.4. Interpolation and extrapolation of median polish effects

$\mu_y(\mathbf{s}_{abc}, t)$ given on Eq. (4) only satisfies the mean value of the cell, so a kind of inter or extrapolation is necessary in order to define the trend component in the location of prediction. For this procedure, a spline type 1 proposed by Cressie (1986) is used, considering the addition of the *Altitude* (w) and *temporal* (t) components. However, temporal component does not require smoothing because the minimum scale of analysis is monthly. Therefore, supposing any location $(\mathbf{s}, t) = (u, v, w, t)$ within a region bounded for a compound of grid lines, i.e. $u_a \leq u < u_{a+1}, v_b \leq v < v_{b+1}, w_c \leq w < w_{c+1}$, and stage time t with $t_1 \leq t < t_n$, where $a \in \{1, \ldots, U-1\}, b \in \{1, \ldots, V-1\}, c \in \{1, \ldots, W-1\}, t \in \{1, \ldots, T\}$; the spatio-temporal trend is usually modeled as follows:

$$
\begin{aligned}
\widehat{\mu}_{mpok}(\mathbf{s}_{abc}, t) = \widehat{\mu} + \widehat{\alpha}_a + \left(\frac{u - u_a}{u_{a+1} - u_a} \right) (\widehat{\alpha}_{a+1} - \widehat{\alpha}_a) + \widehat{\beta}_b + \left(\frac{v - v_b}{v_{b+1} - v_b} \right) (\widehat{\beta}_{b+1} - \widehat{\beta}_b) + \widehat{\xi}_c \\
+ \left(\frac{w - w_c}{w_{c+1} - w_c} \right) (\widehat{\xi}_{c+1} - \widehat{\xi}_c) + \widehat{\tau}_t.
\end{aligned}
$$

For the data out of the grid, Berke (2001) proposed an extrapolation that is extended to the analysis including altitude (w) and time (t). The expression of extrapolation for the trend component is given by:

- For $(\mathbf{s}, t) = (u, v, w, t)$ with $u < u_1, v_1 \leq v_b < v < v_{b+1} \leq v_V, w_1 \leq w_c < w < w_{c+1} \leq w_W$ and $t_1 \leq t \leq t_T$,

$$
\begin{aligned}
\widehat{\mu}_{mpok}(\mathbf{s}_{abc}, t) = \widehat{\mu} + \widehat{\alpha}_1 + \left(\frac{u - u_1}{u_2 - u_1} \right) (\widehat{\alpha}_2 - \widehat{\alpha}_1) + \widehat{\beta}_b + \left(\frac{v - v_b}{v_{b+1} - v_b} \right) (\widehat{\beta}_{b+1} - \widehat{\beta}_b) + \widehat{\xi}_c \\
+ \left(\frac{w - w_c}{w_{c+1} - w_c} \right) (\widehat{\xi}_{c+1} - \widehat{\xi}_c) + \widehat{\tau}_t.
\end{aligned}
$$

- For $(\mathbf{s}, t) = (u, v, w, t)$ with $u_1 \leq u_a < u < u_{a+1} \leq u_U$, $v < v_1$, $w_1 \leq w_c < w < w_{c+1} \leq w_W$ and $t_1 \leq t \leq t_T$,

$$\widehat{\mu}_{mpok}(\mathbf{s}_{abc}, t) = \widehat{\mu} + \widehat{\alpha}_a + \left(\frac{u - u_a}{u_{a+1} - u_a}\right)(\widehat{\alpha}_{a+1} - \widehat{\alpha}_a) + \widehat{\beta}_1 + \left(\frac{v - v_1}{v_2 - v_1}\right)(\widehat{\beta}_2 - \widehat{\beta}_1) + \widehat{\xi}_c + \left(\frac{w - w_c}{w_{c+1} - w_c}\right)(\widehat{\xi}_{c+1} - \widehat{\xi}_c) + \widehat{\tau}_t.$$

- For $(\mathbf{s}, t) = (u, v, w, t)$ with $u_1 \leq u_a < u < u_{a+1} \leq u_U$, $v_1 \leq v_b < v < v_{b+1} \leq v_V$, $w < w_1$ and $t_1 \leq t \leq t_T$,

$$\widehat{\mu}_{mpok}(s_{abc}, t) = \widehat{\mu} + \widehat{\alpha}_a + \left(\frac{u - u_a}{u_{a+1} - u_a}\right)(\widehat{\alpha}_{a+1} - \widehat{\alpha}_a) + \widehat{\beta}_b + \left(\frac{v - v_b}{v_{b+1} - v_b}\right)(\widehat{\beta}_{b+1} - \widehat{\beta}_b) + \widehat{\xi}_1 + \left(\frac{w - w_1}{w_2 - w_1}\right)(\widehat{\xi}_2 - \widehat{\xi}_1) + \widehat{\tau}_t.$$

- For $(\mathbf{s}, t) = (u, v, w, t)$ with $u < u_1$, $v < v_1$, $w_1 \leq w_c < w < w_{c+1} \leq w_W$ and $t_1 \leq t \leq t_T$,

$$\widehat{\mu}_{mpok}(\mathbf{s}_{abc}, t) = \widehat{\mu} + \widehat{\alpha}_1 + \left(\frac{u - u_1}{u_2 - u_1}\right)(\widehat{\alpha}_2 - \widehat{\alpha}_1) + \widehat{\beta}_1 + \left(\frac{v - v_1}{v_2 - v_1}\right)(\widehat{\beta}_2 - \widehat{\beta}_1) + \widehat{\xi}_c + \left(\frac{w - w_c}{w_{c+1} - w_c}\right)(\widehat{\xi}_{c+1} - \widehat{\xi}_c) + \widehat{\tau}_t.$$

- For $(\mathbf{s}, t) = (u, v, w, t)$ with $u < u_1$, $v_1 \leq v_b < v < v_{b+1} \leq v_V$, $w < w_1$ and $t_1 \leq t \leq t_T$,

$$\widehat{\mu}_{mpok}(\mathbf{s}_{abc}, t) = \widehat{\mu} + \widehat{\alpha}_1 + \left(\frac{u - u_1}{u_2 - u_1}\right)(\widehat{\alpha}_2 - \widehat{\alpha}_1) + \widehat{\beta}_b + \left(\frac{v - v_b}{v_{b+1} - v_b}\right)(\widehat{\beta}_{b+1} - \widehat{\beta}_b) + \widehat{\xi}_1 + \left(\frac{w - w_1}{w_2 - w_1}\right)(\widehat{\xi}_2 - \widehat{\xi}_1) + \widehat{\tau}_t.$$

- For $(\mathbf{s}, t) = (u, v, w, t)$ with $u_1 \leq u_a < u < u_{a+1} \leq u_U$, $v < v_1$, $w < w_1$ and $t_1 \leq t \leq t_T$,

$$\widehat{\mu}_{mpok}(\mathbf{s}_{abc}, t) = \widehat{\mu} + \widehat{\alpha}_a + \left(\frac{u - u_a}{u_{a+1} - u_a}\right)(\widehat{\alpha}_{a+1} - \widehat{\alpha}_a) + \widehat{\beta}_1 + \left(\frac{v - v_1}{v_2 - v_1}\right)(\widehat{\beta}_2 - \widehat{\beta}_1) + \widehat{\xi}_1 + \left(\frac{w - w_1}{w_2 - w_1}\right)(\widehat{\xi}_2 - \widehat{\xi}_1) + \widehat{\tau}_t.$$

- For $(\mathbf{s}, t) = (u, v, w, t)$ with $u < u_1$, $v < v_1$, $w < w_1$ and $t_1 \leq t \leq t_T$

$$\widehat{\mu}_{mpok}(\mathbf{s}_{abc}, t) = \widehat{\mu} + \widehat{\alpha}_1 + \left(\frac{u - u_1}{u_2 - u_1}\right)(\widehat{\alpha}_2 - \widehat{\alpha}_1) + \widehat{\beta}_1 + \left(\frac{v - v_1}{v_2 - v_1}\right)(\widehat{\beta}_2 - \widehat{\beta}_1) + \widehat{\xi}_1 + \left(\frac{w - w_1}{w_2 - w_1}\right)(\widehat{\xi}_2 - \widehat{\xi}_1) + \widehat{\tau}_t.$$

Similarly, it can be done for the case in which $u > u_U$, $v > v_V$ and $w > w_W$.

In this way, the forecast requires to project the temporal effect value of the median polish to prediction period t_{T+1} since the vector only covers the sample period of this vector. Then, the ARIMA technique is used, a versatile and practical methodology for treating and forecasting temporal series, that allows the projection of seasonal components for a future period (see details in Chatfield, 2013). In this sense, the temporal effect stays in terms of an ARIMA that is expressed as follows:

$$\widehat{\tau}_{T+1} \approx ARIMA(p, d, q)[P, D, Q]_S \tag{6}$$

where p and P are the autoregressive parameters, q and Q are the moving average parameters, d and D are the differences to remove trend and seasonality, respectively, and S is the seasonal order.

2.5. Ordinary space–time kriging on residuals

Lastly, the MPK prediction corresponds to the sum of the median polish surface plus the surface obtained from the ordinary space–time kriging of the residuals, $\widehat{\delta}_{mpok}(\mathbf{s}, t)$. Then, it is obtained by

$$\widehat{Z}_{mpok}(\mathbf{s}, t) = \widehat{\mu}_{mpok}(\mathbf{s}, t) + \widehat{\delta}_{mpok}(\mathbf{s}, t).$$

Assuming that

$$\widehat{\delta}_{mpok}(\mathbf{s}_0, t_0) = \widehat{\theta}_\delta + \mathbf{c}_\delta' \boldsymbol{\Sigma}_\delta^{-1} \left(\boldsymbol{\delta} - \mathbf{1}\widehat{\theta}_\delta\right), \quad \mathbf{s}_0 \in \mathbb{R}^3,\ t_0 \in \mathbb{Z}$$

where $\mathbf{1} = (1, \ldots, 1)'$, $\boldsymbol{\Sigma}_\delta = \mathrm{Cov}(\boldsymbol{\delta})$, $\boldsymbol{\delta} = \mathbf{Z}_{mpok} - \widehat{\boldsymbol{\mu}}_{mpok}$ with $\mathbf{Z}_{mpok} = (Z_{mpok}(\mathbf{s}_1, t_1), \ldots, Z_{mpok}(\mathbf{s}_n, t_n))'$ and $\widehat{\boldsymbol{\mu}}_{mpok} = (\hat{\mu}_{mpok}(\mathbf{s}_1, t_1), \ldots, \hat{\mu}_{mpok}(\mathbf{s}_n, t_n))'$, $\mathbf{c}_\delta = \mathrm{Cov}(\boldsymbol{\delta}, \delta_0)$ with $\delta_0 = \delta(\mathbf{s}_0, t_0)$, $\boldsymbol{\delta} = (\delta(\mathbf{s_1}, t_1), \ldots, \delta(\mathbf{s_n}, t_n))'$, and $\widehat{\theta}_\delta = \left(\mathbf{1}'\boldsymbol{\Sigma}_\delta^{-1}\mathbf{1}\right)^{-1} \mathbf{1}'\boldsymbol{\Sigma}_\delta^{-1}\boldsymbol{\delta}$ represents the generalized least squares estimator of the mean constant for the residual process $\delta(\cdot)$ based on the spatio-temporal structure of the covariance matrix $\boldsymbol{\Sigma}_\delta$.

The minimized mean squared prediction error ($MSPE$) is the ordinary kriging variance,

$$\begin{aligned} &MSPE(Z(\mathbf{s}_0, t_0), \hat{Z}_{mpok}(\mathbf{s}_0, t_0)) \approx MSPE(\delta(\mathbf{s}_0, t_0), \hat{\delta}_{mpok}(\mathbf{s}_0, t_0)) \\ &\quad = \hat{\sigma}^2_{mpok}(\mathbf{s}_0, t_0) = \sigma^2 - \mathbf{c}_\delta' \boldsymbol{\Sigma}_\delta^{-1} \mathbf{c}_\delta + (1 - \mathbf{1}'\boldsymbol{\Sigma}_\delta^{-1}\mathbf{c}_\delta)^2 / (\mathbf{1}'\boldsymbol{\Sigma}_\delta^{-1}\mathbf{1}) \end{aligned}$$

where $\sigma^2 = \mathrm{Cov}(\mathbf{0}, 0)$ is the sill of the space–time variogram.

2.6. Space–time correlation model

Once verified and removed both the spatial and temporal trends of the data, the interest of the spatio-temporal analysis is given in terms of the empirical estimation of the covariance function, which agree with the hypothesis that stationary will depend only on the spatial ($\mathbf{h}_s = \mathbf{s}_i - \mathbf{s}_{i'}$, $i \neq i', i, i' = 1, \ldots, n$) and temporarily ($h_t = t_i - t_{i'}$) separation of the observations. So, it extends the procedures of the spatial statistics to the temporal domain, and affects all possible combinations with fixed location and variable time, fixed time and variable location, and when both are variables: spatial and temporal effects of the phenomenon.

Given this setting, the product–sum covariance model proposed by De Iaco et al. (2001) is fitted. This model supposes a generalization of the product model, and it is obtained combining sums and products of purely spatial and temporal covariances. Moreover, it is a non-separable model that is also versatile and flexible for spatio-temporal processes that easily fits to a data set. This covariance model is given by

$$C_{st}(\mathbf{h}_s, h_t) = k_1 C_s(\mathbf{h}_s) C_t(h_t) + k_2 C_s(\mathbf{h}_s) + k_3 C_t(h_t) \tag{7}$$

where $C_s(\mathbf{h}_s)$ is the space covariance function, $C_t(h_t)$ is the time covariance function, and $k_1 > 0$, $k_2 \geq 0$, $k_3 \geq 0$ to ensure admissibility.

However, De Iaco et al. (2002) introduced a sum–product generalized covariance model as a function of the variograms, which is given by

$$\gamma_{st}(\mathbf{h}_s, h_t) = \gamma_{st}(\mathbf{h}_s, 0) + \gamma_{st}(\mathbf{0}, h_t) - k\gamma_{st}(\mathbf{h}_s, 0)\gamma_{st}(0, h_t) \tag{8}$$

where $\gamma_{\mathbf{s},t}(\mathbf{h}_s, 0)$ and $\gamma_{\mathbf{st}}(0, h_t)$ are valid spatial and temporal bounded variogram functions, respectively, and

$$k = \frac{sill(\gamma_{st}(\mathbf{h}_s, 0)) + sill(\gamma_{st}(\mathbf{0}, h_t)) - sill(\gamma_{st}(\mathbf{h}_s, h_t))}{sill(\gamma_{st}(\mathbf{h}_s, 0)) \cdot sill(\gamma_{st}(\mathbf{0}, h_t))}$$

where $0 < k \leq 1/max\{sill(\gamma_{st}(\mathbf{h}_s, 0)), sill(\gamma_{st}(\mathbf{0}, h_t))\}$. Note that k is selected in such a way to ensure that the global sill is fitted (De Iaco et al., 2002).

In order to establish the hypothesis of the methodological operation in a hydrogeological basin for practical purposes, we present a four-dimensional scheme for monthly precipitation data in the next section, considering the dimension of the study region and the density of meteorological stations that the interpolator requires for the analysis.

2.7. Goodness of fit model

Cross validation is used for calculating the goodness-of-fit of the estimated precipitation. The method involves omitting an observation and using the remaining data for predicting the observations that are omitted. Therefore, the prediction error may be obtained as the observed value minus predicted value. The repetition of this procedure on a data set of interest allows to know the variability of the prediction error. The procedure is applied to 15% of the data; this percentage is obtained from a stratified sample with a subpopulation made-up by months.

3. Monthly precipitation of a hydrogeological zone in Meta (Colombia)

The precipitation variability in Colombia and the transition zone between the Andean and Orinoquia regions (Eastern Cordillera of Colombia) are determined by the orographic structure that comprises the Andes mountain system, the trade winds influence and the southern oscillation of the intertropical convergence zone (Toma and Webster, 2010). These characteristics define a bimodal rainfall regime for the area, which is characterized by having an extended time period of rain interspersed by dry weather. In January of every year, the Eastern Plains are under the trade winds influence that blow from southwest to northeast, moving the clouds and creating a region of conditions that tends to establish the dry weather. From April to November, the atmospheric depression moves north direction, and the clouds accumulated on the plains cause the highest levels of precipitation.

3.1. Structural design

A monthly precipitation map was generated within an area of approximately 2.567.180 hectares that covers the 30% of the southwest region of the hydrogeological zone of the Meta river (see Fig. 4). A hydrogeological zone is "A set of basins and sub-basins with lithological, structural and geomorphological similar features; it presents a recognizable spatially homogeneous hydrogeological behavior" (Bloomfield et al., 2011). The hydrogeological zone is defined by the Institute of Hydrology, Meteorology and Environmental Studies of Colombia (IDEAM, for its acronym in Spanish) to scale 1:200.000, based on the delineation of geological basins of the National Hydrocarbons Agency of Colombia. According to Ponce (1989), the rainfall is not uniformly distributed neither in space nor in time for basins with surfaces greater than 500.000 hectares, so a space–time analysis should be considered in a region of these characteristics.

This data analysis is based on the monthly precipitation records from January 2000 to January 2010 taken from 102 pluviometric stations operated by the IDEAM. The monitoring network covering this region is irregular due to the physical and meteorological conditions of the different zones, and potential needs of the network users (e.g. agricultural and livestock support, supply irrigation needs, water availability for domestic, industrial and miner uses, among others).

The region is bounded based on the station position in dimensions of 122.604 m (northeast) $\times$ 210.506 m (southwest) and a height ranging from 180 m above sea level (masl) to 3.250 masl. For practical purposes, the area of study is rotated 40° at northeast direction in order to make the sweeps in the east and north spatial directions equivalent to the tables in which the method is based.

According to a spatio-temporal distribution of this four-dimensional data, the data set is divided to $7_u \cdot 6_v \cdot 5_w \cdot 121_t$ four-dimensional cells, the spatial dimensions of this cells are 20.434 m $\times$ 42.101 m $\times$ 767.5 m (see Figs. 5–7).

Due to the regularity in taking records, the number of scenarios for analysis using this technique is 121 months. According to Table 1, each precipitation set has an average of 4.2% of absent values, so

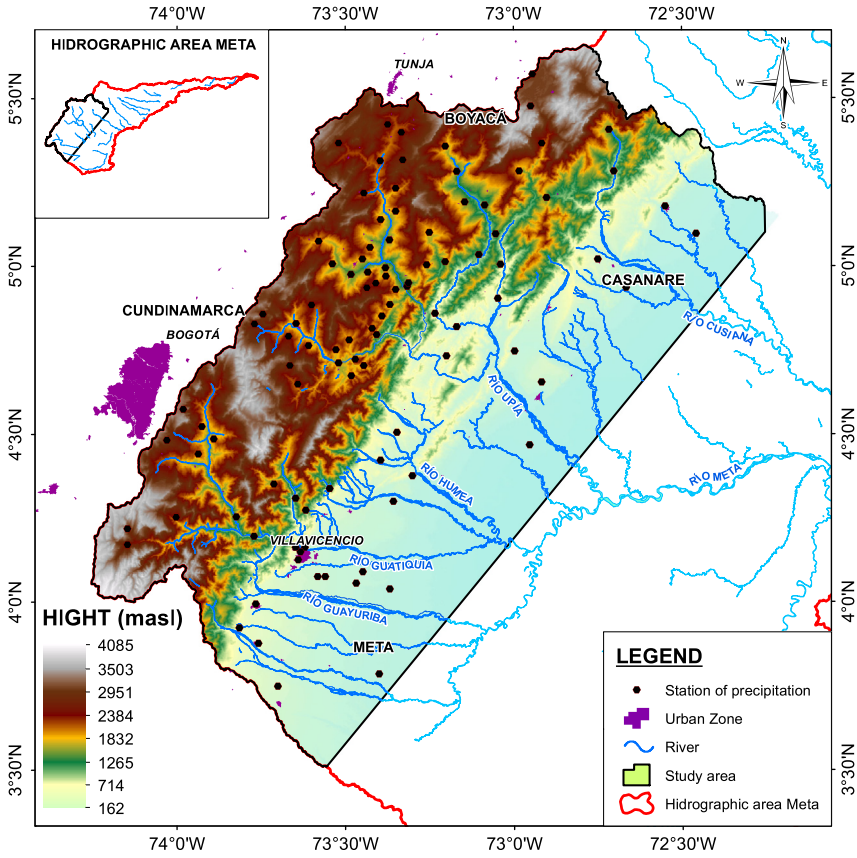

Fig. 4. Meta river hydrogeological zone.

the most extreme case is the series ID 35 095 030 with 30% of missing data. However, the space–time configuration proposed works well for applying the median polish.

3.2. Median polish for a spatio-temporal process

This spatio-temporal exploratory analysis provides a novelty in comparison to classical methods, whose description is made based on statistical resistance. However, although the technique is slightly sensitive to the influence of missing data and observations numerically distant of all other data, square root transformation of the monthly precipitation data is used to stabilize the variance and reduce the potential adverse effects of isolated unusual observations.

For decomposition of the variable in an array of four dimensions, the *ConstructMPst* function in the STMedianPolish library of the R package was used (Martinez et al., 2015). This function creates an object with regular data to use the *MedianPolishM*, a function to employ median polish technique. After using three iterations, the technique gets to stabilize the median in four study directions, and thus, it confronts the assumptions of stationary process.

Following the algorithm for estimation of parameters presented in Section 2.3, we obtain the longitude, latitude and altitude, and time estimation of marginal effects, which are shown in Fig. 8. In Eq. (5), these parameters are estimated through differences between the medians that are given by the square root of the response variable that is given in mm.

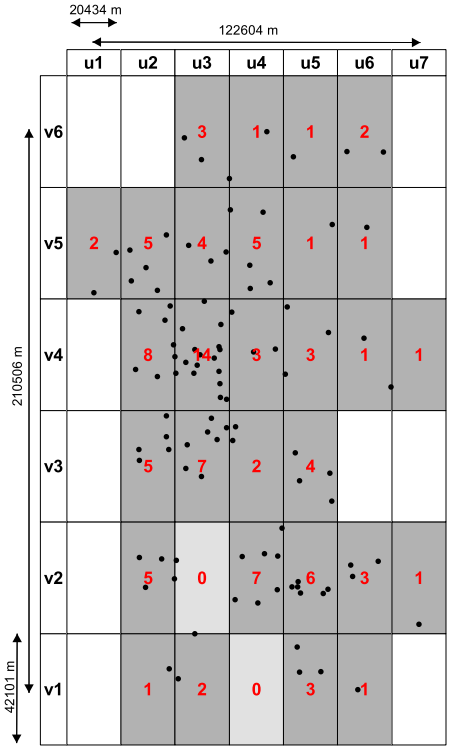

Fig. 5. Trace longitude (u)-latitude (v).

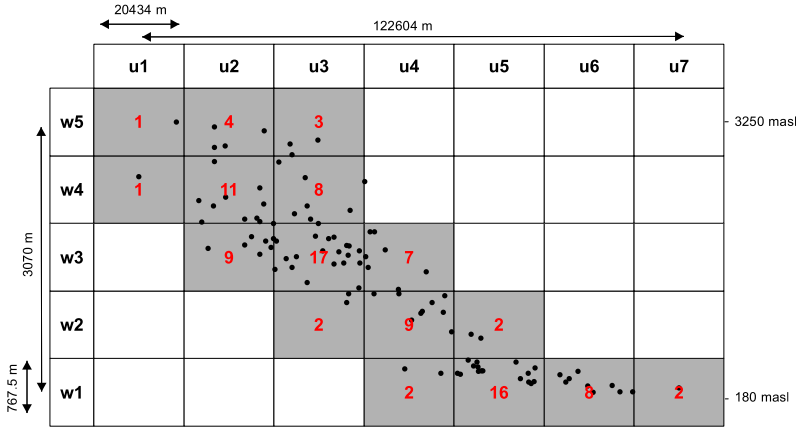

Fig. 6. Trace longitude (u)-altitude (w).

According with Fig. 8, the temporal effects show a seasonal pattern of lower precipitation levels in the first and last months of each year, with higher precipitation in the remaining months and a period less rainy between July and August.

Interpolating the effects *longitude*, *latitude* and *altitude* by means of the *splineMPST* function of STMedianPolish library, the surface which represents the spatial trend associated with the process is

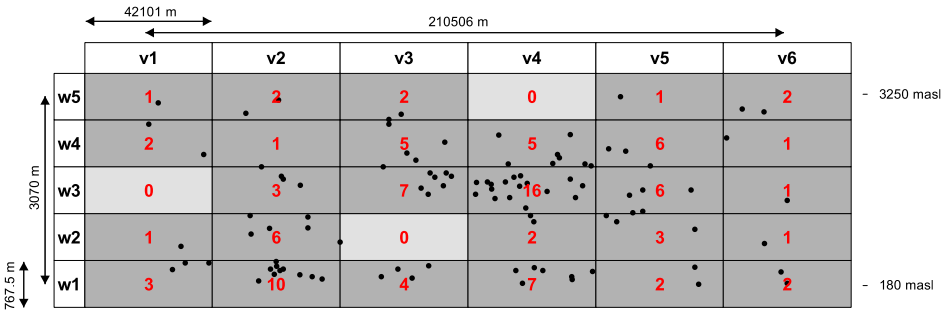

Fig. 7. Trace latitude (v)-altitude (w).

Table 1
Missing data series of monthly precipitation.

ID STATION	NA	ID STATION	NA	ID STATION	NA	ID STATION	NA	ID STATION	NA
35035010	15	35090060	10	35060240	11	35020010	2	35180010	5
35035020	0	35090050	4	35060230	4	35010090	2	35090110	21
35095110	5	35090040	6	35060220	0	35500070	2	35090070	17
35075040	0	35080110	3	35060210	3	35010060	2	35030040	4
35075020	1	35080100	13	35060200	1	35010040	1	35030030	2
35035070	6	35080080	1	35060180	4	35010020	0	35070020	1
35195050	4	35080070	0	35060170	1	35190030	4	35060300	1
35195030	22	35080060	4	35060160	6	35090010	9	35060250	3
35105020	20	35080030	0	35060150	5	35080050	3	35030010	0
35105050	3	35080010	1	35060140	4	35070550	11	35020310	0
35095030	37	35070470	7	35060130	8	35070520	3	35020290	7
35085050	2	35070320	6	35060120	4	35070500	3	35020280	10
35085040	12	35070210	1	35060050	1	35070480	20	35020060	2
35085020	9	35070170	1	35050020	3	35070310	2	35020020	3
35065010	0	35070130	5	35050010	1	35070260	13	35055010	4
35045020	0	35070100	3	35040010	10	35070230	5	35030100	2
35025060	5	35070070	2	35030290	0	35070190	1	35030090	4
35025050	5	35070060	2	35030050	4	35070110	0	35030080	1
35025020	0	35070050	3	35030020	3	35070080	1	35190050	10
35190070	22	35070040	12	35020350	0	35070010	5	35070030	1
35020300	4	35060100	0						

presented in Fig. 9. The orographic dipole of Piedmont Llanero imposes a pattern of higher rainfall that flows in the northwest direction and height precipitation levels over the networks that drain to the Meta River.

3.3. Space–time correlation model for precipitation

In order to remove the spatio-temporal trend from the observations and to calculate the variogram over residuals, we used the *removetrendMPst* function from the STMedianPolish library. Empirical (left) and fitted (right) space–time variogram surfaces for precipitation are shown in Fig. 10. Note that temporal variogram part highlights the annually seasonally presented by the data, this cyclical scheme over the variogram generally is called "undamped hole-effect" (Pyrcz and Deutsch, 2003). Such structure was fitted to the theoretical generalized model proposed by De Iaco et al. (2001). However, it differs in that this combines simultaneously the sine and cosine functions since an empirical model in temporal direction is complex to fit, so the cosine term models the waves with cycles of 12 months, and the absolute value of sine term models the fluctuation of half phase.

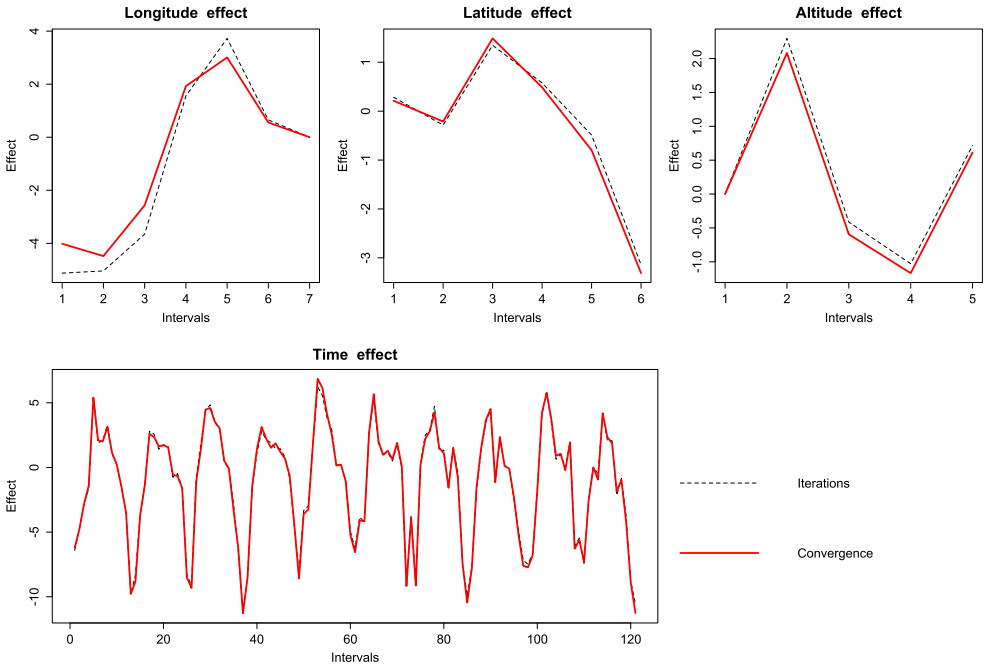

Fig. 8. Estimation of marginal effects obtained using Eq. (5).

Thus, the temporal and spatial functional forms of the variogram are given by

$$\gamma_{st}(\mathbf{h}_s, 0) = 13.7[1 - \exp(-\mathbf{h}_s/13\,900)]$$

$$\gamma_{st}(\mathbf{0}, h_t) = 4\left[1 - \exp\left(\frac{h_t}{29}\right)\right] + 1.57\left[1 - \cos\left(\frac{h_t\pi}{180}\right)\right] + 3.8\left|\sin\left(\frac{h_t\pi}{180}\right)\right|$$

and based on Eq. (8), the spatio-temporal variogram is as follows

$$\gamma_{st}(\mathbf{h}_s, h_t) = 2 + \gamma_{st}(\mathbf{h}_s, 0) + \gamma_{st}(\mathbf{0}, h_t) - 0.07\left[\gamma_{st}(\mathbf{h}_s, 0)\gamma_{st}(\mathbf{0}, h_t)\right].$$

Therefore, the covariance model is given by

$$C_{st}(\mathbf{h}_s, 0) = 13.7\exp(-\mathbf{h}_s/13\,900)$$

$$C_{st}(0, h_t) = 4\exp\left(\frac{h_t}{29}\right) + 1.57\cos\left(\frac{h_t\pi}{180}\right) + 3.8\left|1 - \sin\left(\frac{h_t\pi}{180}\right)\right|$$

and based on Eq. (7), the spatio-temporal covariogram is as follows

$$C_{st}(\mathbf{h}_s, h_t) = 0.07C_s(\mathbf{h}_s)C_t(h_t) + 0.29C_s(\mathbf{h}_s) + 0.002C_t(h_t).$$

3.4. Goodness of fit model

Once the residuals are taken to the original unit of study, the fitted model is evaluated using the leave-p-out cross-validation method. Fig. 11 shows the dispersion graphs of observed vs estimated values by month. Additionally, the coefficients of determination are presented to evaluate the goodness of fit; it is expected that the data will fit the line of 45°.

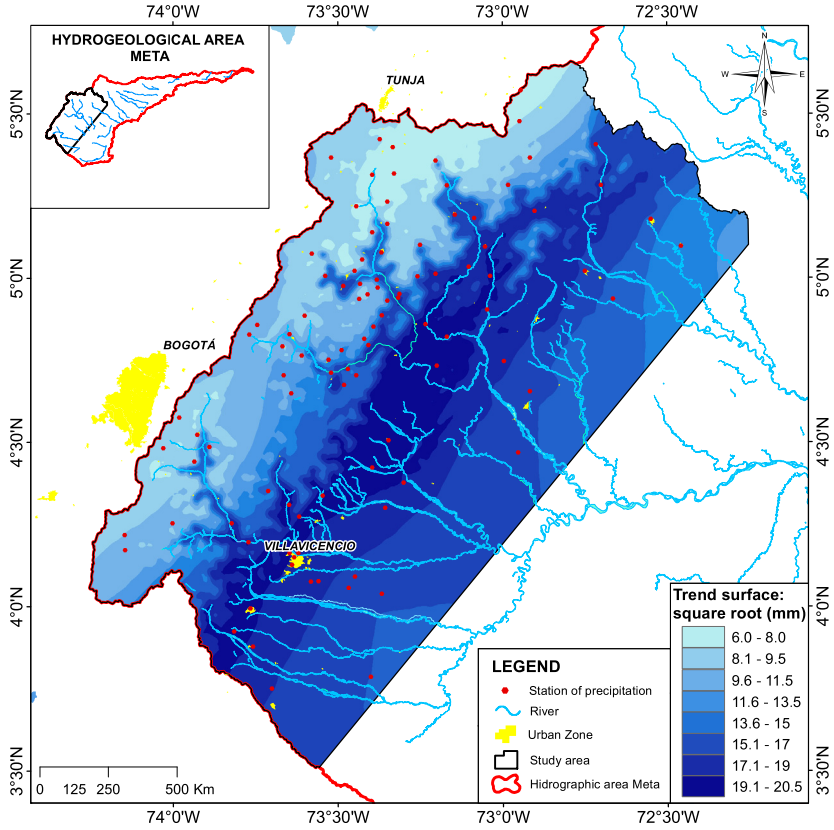

Fig. 9. Spatial trend of precipitation in the study area.

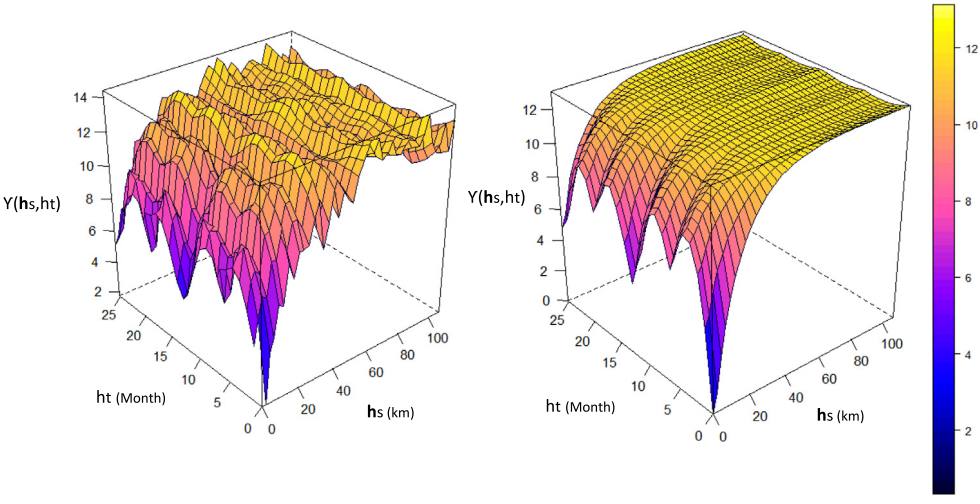

Fig. 10. Empirical (left) and fitted (right) space–time variogram surfaces.

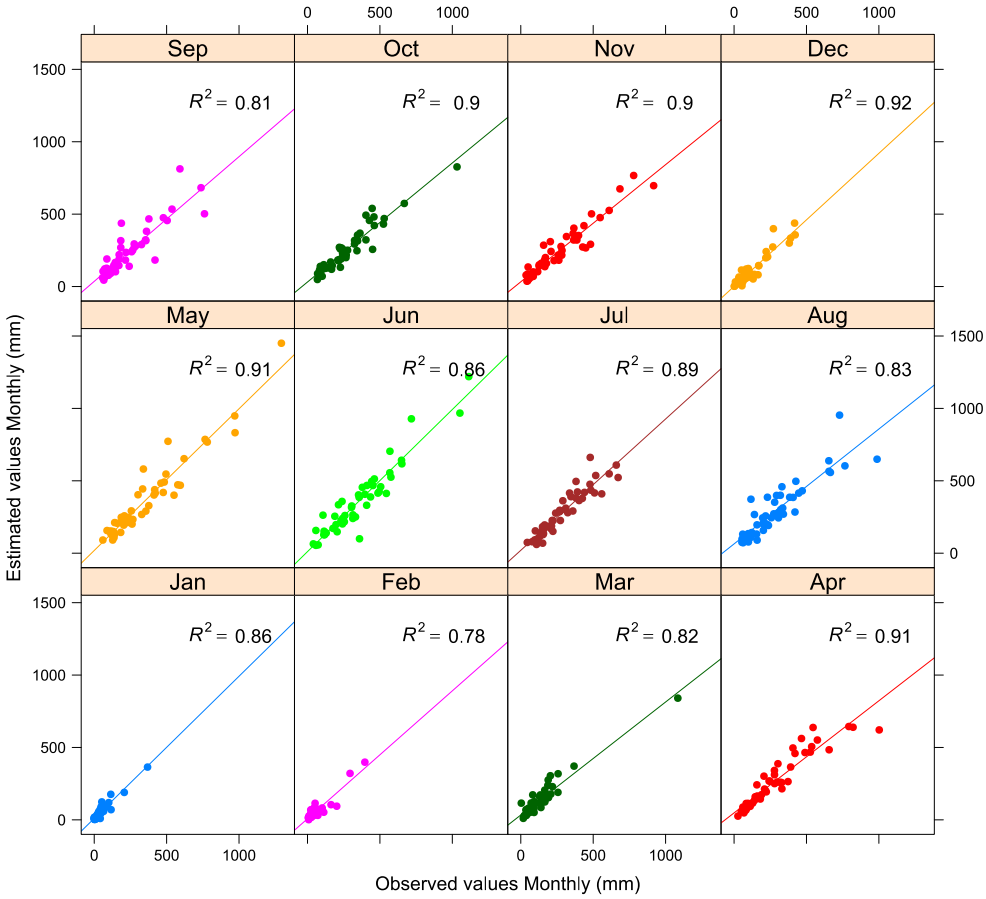

Fig. 11. Monthly cross validation (marginal coefficients of determination, $\boldsymbol{R^2}$).

3.5. Forecast

To illustrate the forecasting, three precipitation maps were generated: one for the rainiest month (June 2008) within the study period, other for the driest month (January 2010) from the last sample period, and finally June 2010, based on projection of the series for temporal effect using the ARIMA methodology.

The ARIMA model used to forecast the temporal effect $\widehat{\tau}_{June2010}$ was $ARIMA(2, 0, 0)[1, 0, 0]_{12}$ with mean zero. The order two for no seasonal autoregressive parameter shows that the endogenous variable (temporal effect) is explained by the observations of two previous periods, and one seasonal first order autoregressive parameter, which shows that the variable also is explained by previous observations with lags of 12 periods. Fig. 12 shows the temporal effect for the 2011 period together with its confidence bands to the 95% confidence level (light gray).

Regardless of the rainy situation selected (June 2008 or June 2010), the higher levels of rainfall are distributed through the Cordillera limit and eastern plains (see Fig. 13). A strong concentration upstream of Guatiquía and Guayuriba rivers in Villavicencio Meta city is marked. As it descends southeastward, the rainfall fringe of Piedmont becomes an area of low rainfall; this kind of rainfall is called orographic rainfall, which is produced by the rise of a moist air column up-slope on orographic barrier, like a mountain. In this rise, the air is cooled to a dew point temperature and relative humidity of 100%, which causes rain (Álvarez-Rodriguez, 2011).

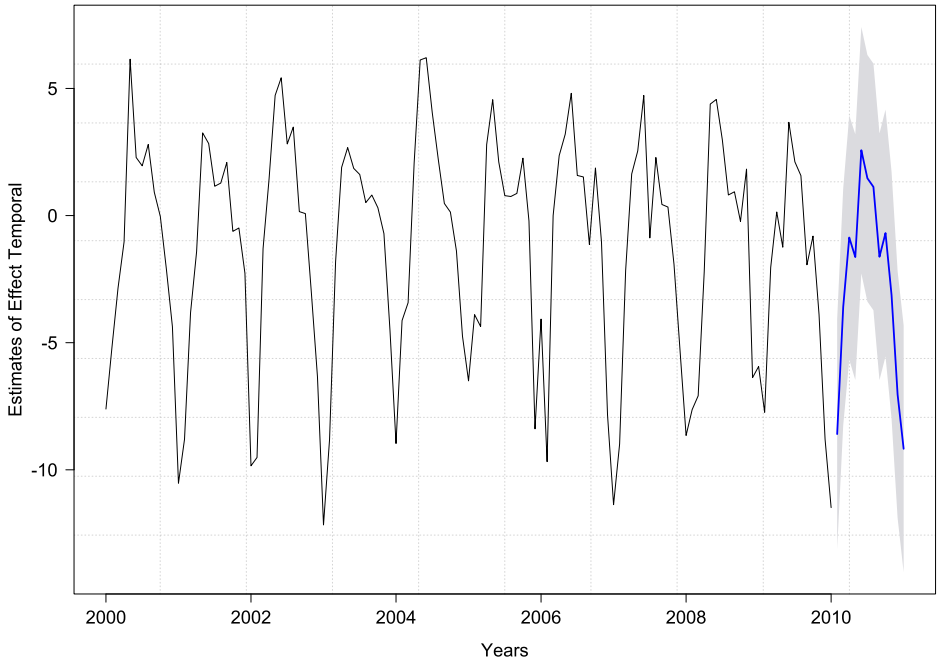

Fig. 12. Temporal prediction effect for the 2011th year with its confidence region (light gray region).

In order to support the work with MPK for space–time analysis, MPK provides a standard error map that shows the uncertainty related to the predicted values for June 2008, January 2010 and June 2010 (see Fig. 13 (right maps)). The error increases in southeastward direction and best predictions zones are around concentrations of spatial observations, showing the method depends too much on spatial data configuration. On the other hand, map prediction of June 2010 shows a range of deviations higher in respect to other maps because this period is not part of the time sample. The cross validation allows to visualize the quality of forecast within a sample period (January 2000 to January 2010); however, it is necessary to have the observed data captured for the same 102 meteorological stations and contrast them with the fitted values (see Fig. 14).

Considering a linear relation between forecast and observed values, the fitted model is evaluated through the determination coefficient, which is 0.75. Although the linear association is practically strong, a slight inclination of points cloud is evidenced because they show a mean for June 2010 below the actual values. This could be an error in the estimation; however, for that period, Colombia faced a weather phenomenon called "*La niña*" (NOAA, 2014), a recurrent but not periodic phenomenon that brings monthly average rainfall higher than the normal levels (Cepal and BID, 2012).

4. Conclusions

In this paper, a robust and resistant technique to generate the rainfall maps is proposed, which comes from irregularly spaced monitoring stations and considers the joint progress of a process in space–time. However, regardless of the efficient of the technique in four dimensions, the precipitation variability could be related to other spatial covariates; for instance, slope, vegetation cover, the distance with respect to the coast (for studies with coastal boundaries), among others. This suggests an addition of covariates to the trend analysis, which could be material available in digital elevation models for future papers.

The MPK methodology was generalized in order to include the spatio-temporal coordinates as covariates. Moreover, regardless of the irregular spatial configuration of the station locations, monthly

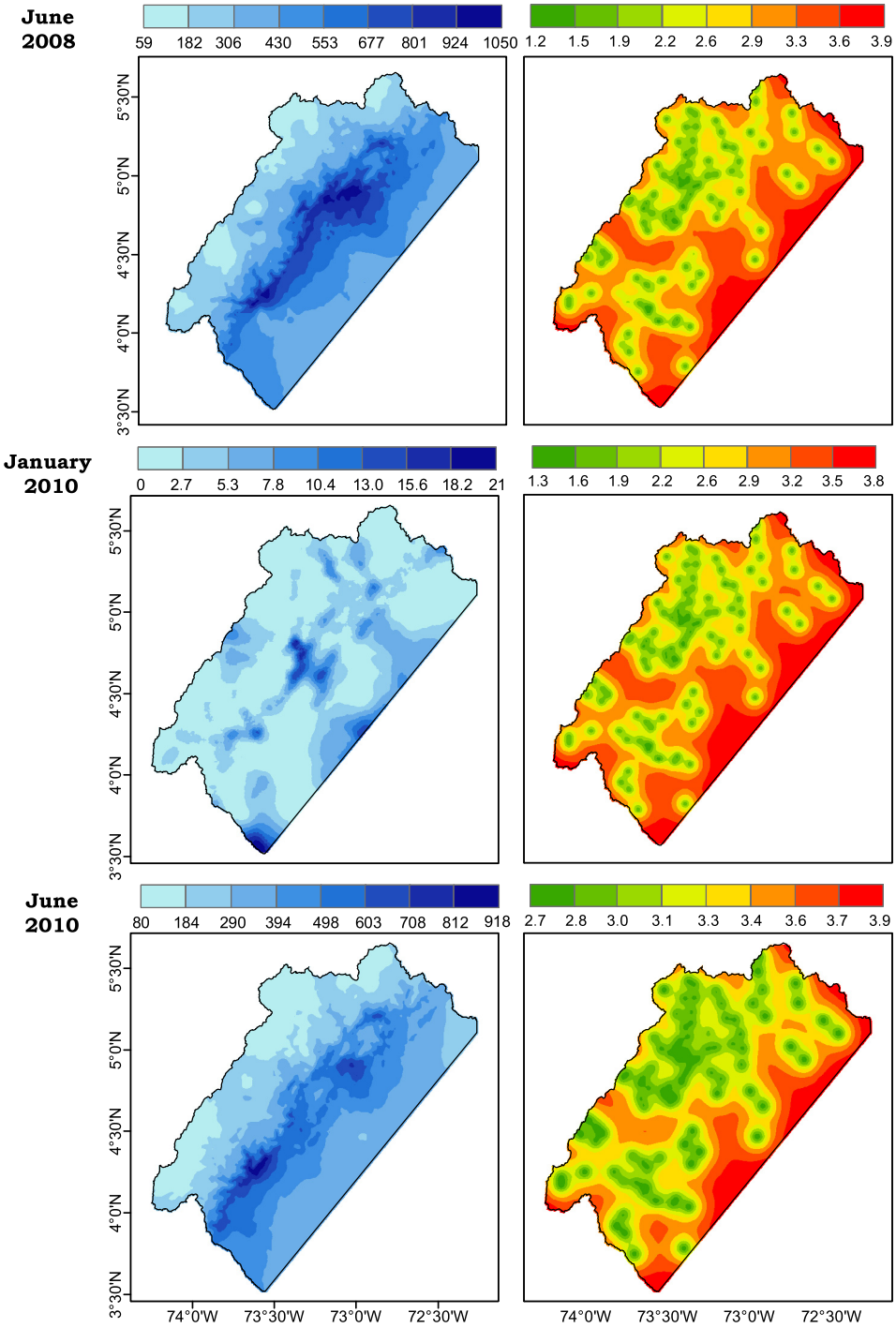

Fig. 13. Monthly rainfall prediction maps (left) and monthly error maps (right).

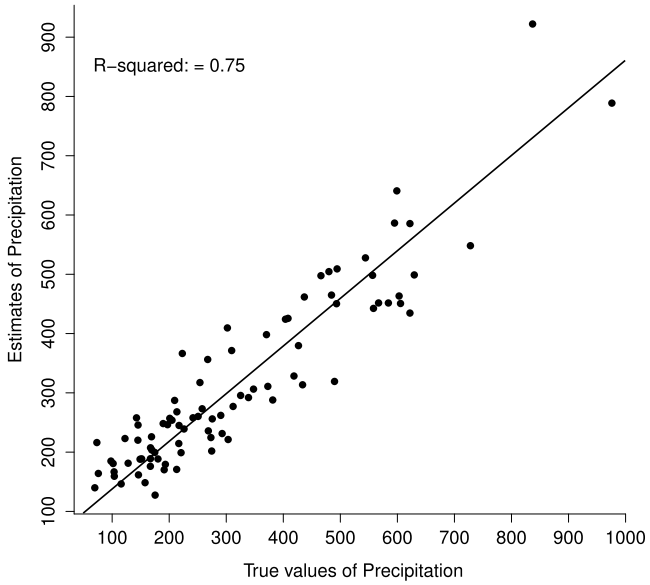

Fig. 14. Comparison between observed and fitted values for June 2010.

rainfall measures were considered after using a median polish in four dimensions (latitude, longitude, altitude and time, (u, v, w, t)) as a realization of a random function in space and time, whose correlation structure was fitted using a sum–product generalized model.

From a practical point of view, the median polish for multiple covariates was an efficient technique in the trend fitted model from the spatio-temporal position of the sample study. The main advantage of MPK in four dimensions is the robust fit of the smooth and flexible trend surface. Furthermore, in our application, the error maps from MPK in four dimensions were small, but the reasons for this have not yet been investigated.

Acknowledgments

Work was partially funded and supported by Applied Statistics in Experimental Research, Industry and Biotechnology (Universidad Nacional de Colombia) (COL0004469), and by Core Spatial Data Research (Faculty of Engineering, Universidad Distrital Francisco José de Caldas) (COL0013969). We thank the AE and three reviewers for providing helpful comments on an earlier version of the manuscript.

Appendix A. Supplementary data

Supplementary material related to this article can be found online at http://dx.doi.org/10.1016/j.spasta.2016.10.003. These data include the Google map of the most important areas described in this article.

References

Álvarez-Rodriguez, J., 2011. Estimación de la distribución espacial de la precipitación en zonas montañosas mediante métodos geoestadísticos (Ph.D. thesis), E.T.S.I. Caminos, Canales y Puertos (UPM).

Berke, O., 2001. Modified median polish kriging and its application to the Wolfcamp-Aquifer data. Environmetrics 12 (8), 731–748.

Berke, O., 2004. Exploratory disease mapping: kriging the spatial risk function from regional count data. Int. J. Health Geograph. 3 (18), 1–11.

Bloomfield, J.P., Bricker, S.H., Newel, A.J., 2011. Some relationships between lithology, basin form and hydrology: a case study from the Thames basin, UK. Hydrol. Process. 25 (16), 2518–2530.
Cepal, , BID, , 2012. Valoración de daños y pérdidas. Ola invernal en Colombia, 2010–2011. Tech. rep. Comisión Económica para América Latina y el Caribe.
Chatfield, C., 2013. The Analysis of Time Series: An Introduction. CRC Press, London.
Cressie, N., 1986. Kriging nonstationary data. J. Amer. Statist. Assoc. 81 (395), 625–634.
Cressie, N.A.C., 1991. Statistics for Spatial Data. Jhon Wiley & Sons, New York.
Cressie, N.A.C., Wikle, C.K., 2011. Statistics for Spatio-Temporal Data. John Wiley & Sons, New Jersey.
De Iaco, S., Myers, D.E., Posa, D., 2001. Space–time analysis using a general product-sum model. Statist. Probab. Lett. 52 (1), 21–28.
De Iaco, S., Myers, D.E., Posa, D., 2002. Space–time variograms and a functional form for total air pollution measurements. Comput. Statist. Data Anal. 41 (2), 311–328.
Hoaglin, D.C., Mosteller, F., Tukey, J.W., 2000. Understanding Robust and Exploratory Data Analysis. John Wiley & Sons, New York.
Hoaglin, D.C., Mosteller, F., Tukey, J.W., 2011. Exploring Data Tables, Trends, and Shapes. John Wiley & Sons, New Jersey.
Lee, D.J., Durbán, M., 2011. P-spline ANOVA-type interaction models for spatio-temporal smoothing. Stat. Model. 11 (1), 49–69.
Luo, Z., Wahba, G., Johnson, D.R., 1998. Spatial–temporal analysis of temperature using smoothing spline ANOVA. J. Clim. 11 (1), 18–28.
Martinez, W., Melo, C.E., Melo, O.O., 2015. STMedianPolish: Spatio-Temporal Median Polish. R package version 0.2.
Martínez-Ruiz, F., 2008. Modelización de la función de covarianza en procesos espacio-temporales: análisis y aplicaciones (Ph.D. thesis), Universitat de València.
Mohanty, B.P., Kanwar, R.S., 1994. Spatial variability of residual nitrate-nitrogen under two tillage systems in central Iowa: A composite three-dimensional resistant and exploratory approach. Water Resour. Res. 30 (2), 237–251.
NOAA, 2014. What are El Niño and La Niña? National Ocean Service. URL http://oceanservice.noaa.gov/facts/ninonina.html.
Ponce, V.M., 1989. Engineering Hydrology: Principles and Practices. Prentice Hall, Hardcover.
Pyrcz, M.J., Deutsch, C.V., 2003. The whole story on the hole effect. Geostatistical Association of Australasia, Newsletter 18.
Rekabi, F.A., El Sheikh, A., 2013. Improved median polish kriging for simulation metamodeling. ArXiv e-prints (arXiv:1307.8172). URL http://adsabs.harvard.edu/abs/2013arXiv1307.8172R.
Sun, Y., Genton, M.G., 2012. Functional median polish. J. Agric. Biol. Environ. Stat. 17 (3), 354–376.
Toma, V.E., Webster, P.J., 2010. Oscillations of the intertropical convergence zone and the genesis of easterly waves. Part I: diagnostics and theory. Clim. Dynam. 34 (4), 587–604.
Tukey, J.W., 1977. Exploratory Data Analysis. Addison-Wesley, New Jersey.